XL CILAMCE
IBERO-LATIN AMERICAN CONGRESS ON COMPUTATIONAL METHODS IN ENGINEERING
NOVEMBER 11-14, 2019
Praiamar Natal Hotel & Convention
Natal, RN-BRAZIL

A NUMERICAL 3D MODEL OF SFRC PIPES: PARAMETRIC STUDY OF THE STRENGTH CAPACITY.

Facundo L. Ferrado
Mario R. Escalante
ferradof@frcu.utn.edu.ar
escalam@frcu.utn.edu.ar
Grupo de Investigación en Mecánica Computacional y Estructuras, Universidad Tecnológica Nacional-Facultad Regional Concepción del Uruguay
Ing. Pereyra 676, 3260 Concepción del Uruguay, Argentina, gimce@frcu.utn.edu.ar
Viviana C. Rougier
rougierv@frcu.utn.edu.ar
Grupo de Investigación en Mecánica Computacional y Estructuras, Universidad Tecnológica Nacional-Facultad Regional Concepción del Uruguay
Ing. Pereyra 676, 3260 Concepción del Uruguay, Argentina, gimce@frcu.utn.edu.ar

Abstract. The incorporation of steel fibers to concrete is beneficial from the structural point of view, giving place to the use of the composite material called Steel Fiber Reinforced Concrete (SFRC) in several applications, among which concrete pipes are found. The main contribution of the fibers is their ability to improve the tensile strength and tenacity of plain concrete. This contribution depends mainly on the geometric characteristics and mechanical properties of the fibers, the amount incorporated and the properties of the cement matrix itself. All these factors together will determine the mechanical performance of the structural piece under consideration. This work contributes to a better understanding of the mechanical behavior of this composite material applied to pipes through a parametric study of the strength capacity of pipes considering variations in the dosage and type of fibers as well as variations in the concrete class used. The fibers are represented as discrete elements and randomly distributed in the concrete mass whose characteristics are adopted from fibers available in the local market. The proposed model is simulated in combination with the Monte Carlo method in order to obtain average probabilistic values of strength capacity of pipes, considering the variability of the orientation and distribution of steel fibers within the concrete mass. The maximum load values are obtained by simulating the three edge bearing test (TEBT) according to the IRAM 11503 standard, which is implemented in a finite element analysis tool (ABAQUS®). A constitutive model of damage-plasticity was used for plain concrete and a model of steel for the fibers which takes into account the pull-out phenomenon. Finally, results of the simulations are shown through tables of maximum loads, load-displacement curves and histograms.

Keywords: SFRC, Concrete pipes, Monte Carlo method, Parametric analysis, Discrete modelling.

1 Introduction

The use of SFRC for manufacturing concrete pipes implies a series of improvements related to the performance of this new material both from a technical and economic point of view. With the addition of metallic fibers, an appreciable improvement of several mechanical properties of the concrete is achieved e.g. ductility, toughness. In addition, the combination of reinforced concrete and fibers leads to a positive structural synergy: the bars develop the main resistant function, while the fibers sew the entire surface of the cracks. This prevents crack propagation and also allows to reduce (and even suppress) the use of steel meshes, which require special bending and use of specific machinery for its placement [1] [2] [3].

The main factors influencing the mechanical performance of SFRC are the amount of fibers (dosage), their slenderness (length/diameter ratio) and the quality of the concrete matrix. For the same fiber content, and assuming that the fibers have the same length, the slender fibers are more efficient since there is a greater amount of fibers leading to a better distribution of stresses. [4].

Another important element of the SFRC performance is the orientation and distribution of the fibers in the concrete mass in relation to the direction of the principal stresses. These parameters depend, among others, on concrete slump, framework shape, casting direction, and compaction methods [5]. Thus, an alignment in the same direction of the maximum principal stresses will offer greater efficiency resulting in greater post-crack resistance in relation to a random orientation, while an alignment perpendicular to the direction of the maximum principal stresses would not provide any resistance contribution [6].

Several authors [7] [8] [9] [10] have addressed this topic at material level, analyzing the causes of changes in fiber orientation and distribution and the influence that these changes have on various properties of the material, but there are a few papers in the current literature about how these changes affect mechanical performance of the structural element studied here. In this sense, several predictive models have been developed about the positioning and number of fibers found in critical sections of the structural member [11] [12] [13]. However, these models are designed for self-compacting concrete. For this concrete, the effects of the different types of vibration and direction of the casting flow on the orientation and distribution of the fibers are better known. In addition, most of these models are based on laboratory specimens and not on full-scale structures and, as already mentioned, the shape and size of molds and framework have an important influence on fiber distribution.

At the same time, other authors who have studied structural elements such as slabs and thin-walled elements concluded that although the type of fiber influences the distribution and orientation, the geometry of the structural element seems to be the main factor to be considered. [14] [15].

According to this findings, and in order to provide a tool for those cases where there is no greater control of the orientation and distribution of the fibers, a 3D model of SFRC applied to drainage pipes is proposed, in which the fibers are represented as discrete elements and randomly distributed.

As already said, the factors which have the greater influence in the mechanical performance of SFRC are the dosage and the slenderness of the fibers together with the quality of the concrete itself. So, this factors are chosen to perform a parametric analysis carrying out a sensibility study of the bearing capacity of the pipes, as will be described in the following sections.

Previously, the authors addressed the problem through a 2D model in which the properties of the composite material were found using the theory of mixtures. The material was represented as an equivalent homogeneous material with average properties according to its components (concrete and fibers) [16]. Then, SFRC was described using a damage - plasticity model considering different behaviors in tension and compression using uniaxial stress - strain curves [17]. In the first stochastic study carried out, both the distribution and orientation of the fibers were considered by modifying the properties of each element of the finite element mesh according to the amount of fibers that go through the elements. So, the volume proportion of fibers is obtained for each element and with this proportion, the properties of the equivalent homogeneous material are calculated [18]. Finally, a 3D model was adopted where SFRC was still considered as a homogeneous material using constitutive relationships designed for this composite material [19] until this work, where the fibers are considered as discrete entities within the concrete mass, is reached.

2 NUMERICAL MODEL

2.1 Modelling concept

In a previous work [19] the SFRC composite material was represented as a homogeneous material. In the present work, a 2-phase approach is used to model the behavior of SFRC: the plain concrete is defined and then the fibers are introduced as wire elements (truss). This 2-phase 3D model (see figure 1) is used to perform a nonlinear finite element analysis. The SFRC pipes studied have an internal diameter of 600 mm, wall thickness of 75 mm and a length of 1000 mm.

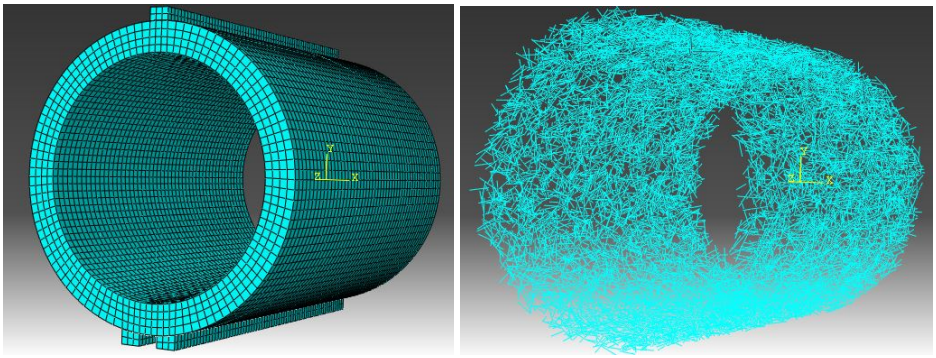

Figure 1. Finite element two-phase modelling concept. Left: concrete pipe. Right: steel fibers.

2.2 Material properties

To represent concrete behavior, the Concrete Damaged Plasticity (CDP) model included in ABAQUS is used. It is assumed that the main two failure mechanisms are tensile cracking and compressive crushing of the concrete material. Thus, the model considers different behaviors under this two solicitations. Under uniaxial tension the stress-strain response is linear elastic until the value of the failure stress is reached. Beyond the failure stress, the formation of micro-cracks is represented macroscopically with a softening stress-strain response. Under uniaxial compression, the response is linear up to the value of initial yield. In the plastic regime the response is typically characterized by stress hardening followed by strain softening beyond the ultimate stress. Figure 2 shows both the typical response of concrete under uniaxial tension and compression according to the CDP model.

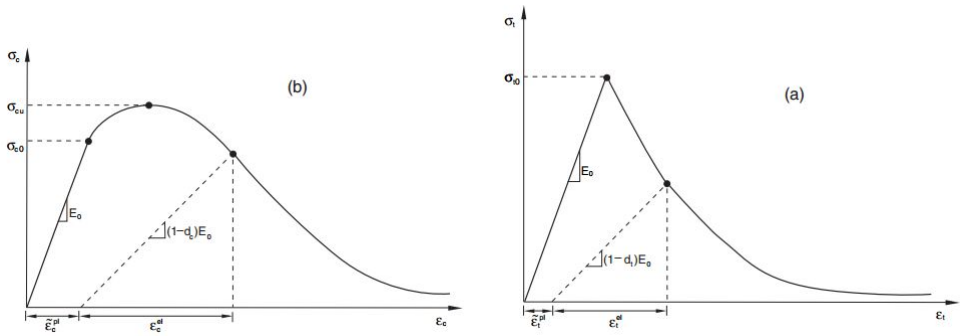

Figure 2. Concrete response under uniaxial loads. Left: compression. Right: tension.

This representation, although somewhat simplified, highlights the main features of the concrete behaviour. A more detailed description of this model can be found in the work [17]. The plasticity parameters adopted are detailed in Table 1.

Thus, to represent the behavior of plain concrete, the uniaxial stress-strain curves for compression and tension must be defined. A constitutive model proposed by the FIB MODEL CODE 2010 is used

Parameter	Dilation Angle	Viscosity	Excentricity	$\sigma_{co}/\ \sigma_{bo}$	K_c
Value	36.31°	0	0.1	1.16	0.67

Table 1. CDP model plasticity parameters.

here. For compression, this model proposes the stress-strain diagram shown in Figure 3.

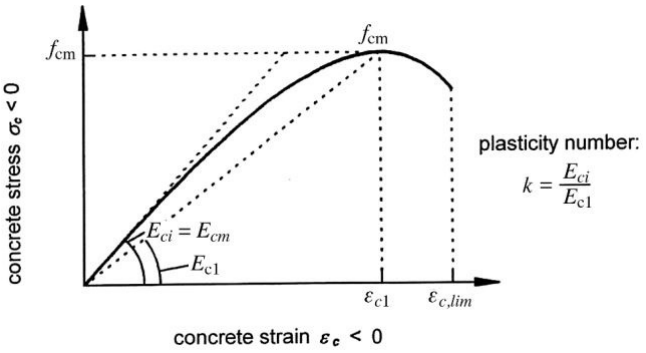

Figure 3. Stress-strain curve for uniaxial compression according to FIB MODEL CODE 2010.

The descending branch of the curve can be approximated as a straight line, as shown in Figure 4.

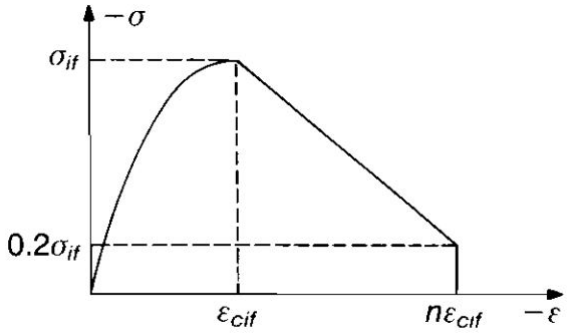

Figure 4. Stress - strain descending branch approach according to FIB MODEL CODE 2010.

Four different concrete classes were adopted here for the parametric analysis: C20, C25, C30 and C35. The parameters required for implementing the compression model and the adopted values for each concrete class are detailed in Table 2.

Concrete Class	Charact. Compr. Str. (MPa)	Elastic Modulus (Mpa)	Strain at max stress (mm)	Peak strain coef.	Plasticity number
C20	20	22610	0.0021	3	2.28
C25	25	25279	0.0022	2.75	2.15
C30	30	28149	0.0023	2.5	2.04
C35	35	29910	0.0023	2.25	1.92

Table 2. Adopted values for concrete compression model.

The finite element software used here requires in its CDP model that, for the compression curve, the deformation values are expressed in terms of inelastic deformation, which is given by the total deformation minus the elastic deformation. Taking this into account, the stress-strain compression curves used in the model are shown in Figure 5.

In a similar way, and for the uniaxial tensile behavior, a tension-crack opening bilinear approximation according to Figure 6 is used.

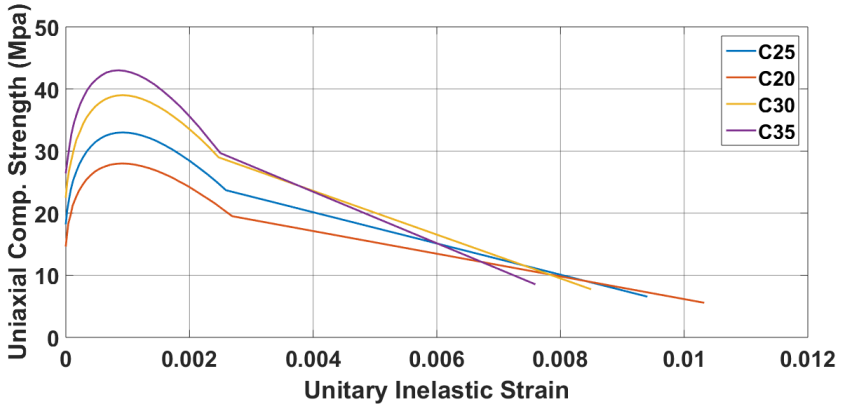

Figure 5. Stress-strain compressive curves used in the finite element model.

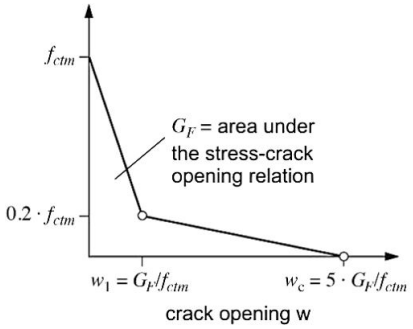

Figure 6. Stress - crack opening displacement tensile curve according to FIB MODEL CODE 2010.

The parameters required by the model are: elastic modulus (E_c), tensile strength (f_{ct}) and fracture energy (G_F) which, in the absence of experimental values, can be estimated from the following expressions based on compressive strength, which was determined experimentally:

$$E_c = 0.043 \cdot 2400^{1.5} \cdot \sqrt{f_c} \quad \text{(MPa)} \tag{1}$$

$$f_{ctm} = 0.3 \cdot f_{ck}^{2/3} \quad \text{(MPa)} \tag{2}$$

$$G_F = 73 \cdot f_{cm}^{0.18} \quad \text{(N/mm)} \tag{3}$$

The adopted values for the above mentioned parameters are summarized in Table 3.

Concrete Class	Tensile Strength (MPa)	Fracture Energy (N/mm)
C20	2.21	0.1329
C25	2.56	0.1369
C30	2.96	0.1405
C35	3.21	0.1436

Table 3. Adopted values for concrete tensile model.

Figure 7 shows the stress-displacement curves in uniaxial tension adopted for the model.

Regarding the steel fibers, an approach proposed by the authors Soetens and Mathys [20] based on the pull-out behavior of a single fiber is used. The main parameters influencing pull-out are implemented through a semi-analytical model described by Van Gysel [21]. This model provides the relationships between pull-out and fiber slip. However, these load-slip curves cannot be implemented in the finite element model directly, so both the values of pull-out and slip loads must be converted into equivalent stress-strain curves.

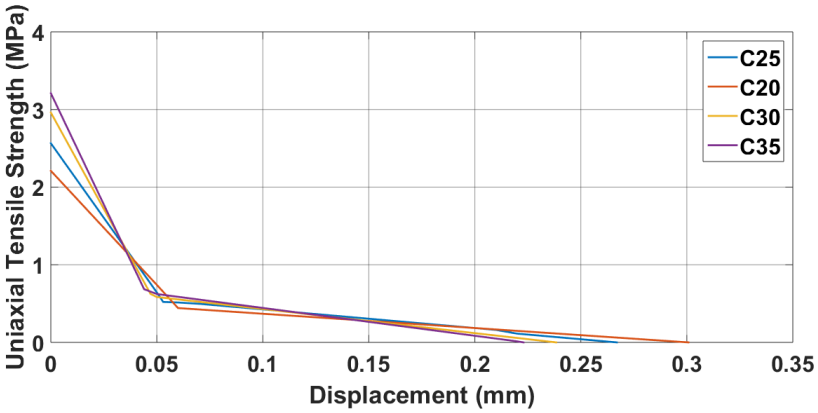

Figure 7. Stress - displacement tensile concrete curves used in finite elements model.

Pull-out-slip load curves can be transferred to equivalent stress-strain curves through the following equations:

$$\epsilon_{eq} = \frac{w}{L_f} \cdot \cos\theta(w) \tag{4}$$

$$\sigma_{eq} = \frac{F_u}{A_f} \cdot \left(\frac{1}{\cos\theta(w)}\right) \tag{5}$$

in which the variable pull-out direction is given by:

$$\theta(w) = \arctan\left(\frac{L_f \cdot \sin(\theta_0)}{L_f \cdot \cos(\theta_0) + w}\right) \tag{6}$$

where w represents the pull-out distance considered equivalent to a crack width, L_f is the initial length of each fiber, F_u is the pull-out load, A_f is the cross section of the fiber and θ_0 is the initial fiber inclination angle that will be discussed next.

To consider the orientation of the fibers in the numerical model, a mathematical formulation proposed by Laranjeira [5] is used. In this formulation, the fiber orientation is based on an initial orientation angle (θ_0) which is a base parameter that defines the mean value and standard deviation of all orientation angles of the individual fibers. This angle varies between 0º for a fiber aligned in the direction of the maximum principal stress and 90º for a fiber parallel to the crack plane, without any contribution to the resistant capacity. Based on data found in the literature [12] [22] [23] [24] and taking into account that representing the mean value and the standard deviation of the orientation angles of all fibers through a truncated Gaussian distribution have a good correlation with the orientation of the fibers experimentally determined, an initial orientation angle of θ_0 = 45º is used in the model. In regard to the pull-out load, this is calculated from the following formula [25] based on the fiber-matrix bond strength τ_{av}.

$$\tau_{av} = \frac{F_u}{\pi \cdot d_f \cdot L_E}, \tag{7}$$

where d_f is the fiber diameter and L_E is the embedded length of the fiber in the matrix. The concept of embedded length has been introduced here since, in order to calculate the contribution of the fibers that cross the cracks, their length, effectively embedded in concrete must be taken into account. The embedded length can vary from 0 to the maximum embedded fiber length (L_E max). This length depends on the bond mechanisms existing along the fiber-matrix interface. The main fiber-matrix resistant mechanism in hooked end fibers is the mechanical anchorage provided by such hooks. Taking these concepts into account, an average value given by the expression provided by Laranjeira [10] is adopted, while as an alternative to the experimental determination of the fiber-matrix bond strength, the expression given by [26] are used . The values adopted are shown in Table 4.

Two different fibers were studied here whose properties are detailed in Table 5.

Fiber geometry	L_E max (mm)	L_E average (mm)	Bond Strength (MPa)
Straight	L/2	L/4	$\tau = 0.396 \cdot \sqrt{f'c}$
Hooked end	L - 7.5	L - 7.5/2	$\tau = 0.825 \cdot \sqrt{f'c}$

Table 4. Embedded lengths and fiber-matrix bond strength values.

Fiber	WIRAND FF1	WIRAND FF3
Length	50 mm	50 mm
Diameter	1 mm	0.75 mm
Cross sectional area	0.785 mm^2	0.441 mm^2
Steel Tensile Strength	1100 MPa	1100 MPa
Elastic Modulus	210000 MPa	210000 MPa
Fibers per Kg	3244	5767
Fiber Type	Hooked end	Hooked end

Table 5. Fiber properties.

2.3 Generation of steel fibers

The Monte Carlo method is used to determine the position of the fibers considering the randomness of their distribution and orientation within the mixture. It is considered that the location of each fiber of length l_f is perfectly determined by the coordinates of its midpoint O' and its direction vector. The coordinates of the midpoint (u, v, w) expressed in cylindrical coordinates gives their location, and the pair of angles (θ, ϕ), with $0 \leq \theta \leq \pi$ and $0 \leq \phi \leq 2\pi$, determine the orientation of the fiber. Figure 8 shows these parameters in a coordinate system.

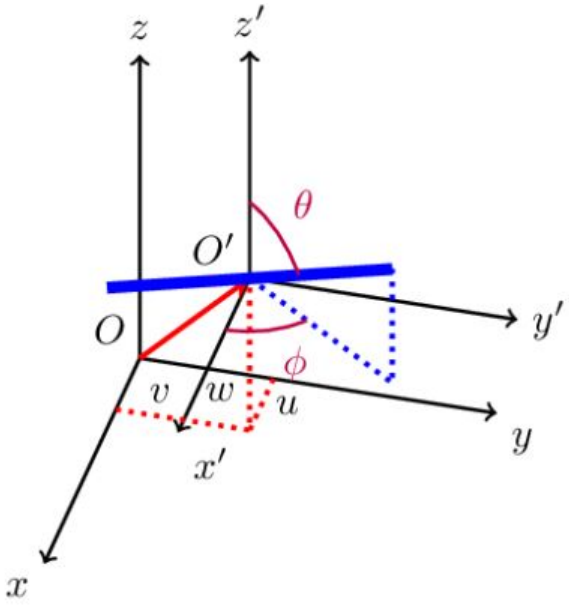

Figure 8. Coordinate system for steel fibers.

From the amount of fibers by weight per volume of concrete to be incorporated (kg/m^3), and considering both the number of fibers per kilogram according to the manufacturer's information and the volume

of concrete necessary to cast a pipe, the number of fibers for a single pipe is determined. This number of fibers will serve as an input parameter of a sampling algorithm developed by the authors themselves through the programming language Python with which the position and orientation of each fiber within the pipe are randomly drawn. When a fiber is raffled, the algorithm checks that this fiber does not intersect any of the fibers already generated. If this happens, the last fiber is discarded and another one is generated, until reaching the necessary number according to the number referred to.

It is mentioned that four different fiber dosages are assessed: 15, 20, 25 and 30 kg/m^3. Considering this dosages, we have different number of fibers per pipe for each fiber type. These number of fibers are summarized in Table 6 .

Fiber dosage (kg/m^3)	WIRAND FF1	WIRAND FF3
15	7739	-
20	10500	18666
25	12895	-
30	15473	-

Table 6. Number of fibers in a single pipe according to fiber dosage and fiber type.

2.4 Three edge bearing test simulation

A bi-phase tridimensional model was constructed to simulate the TEBT. The model consists of the upper loading strip, lower supporting strips, and the concrete pipe. For meshing the concrete pipe 8-node linear brick with reduced integration elements were used (C3D8R) whereas 2-node linear 3-D truss elements for meshing the fibers (T3D2). The interaction between the concrete pipe and the fibers was set as an embedded constraint which is used to specify that an element or group of elements is embedded in "host" elements. In this type of constraint, if a node of an embedded element lies within a host element, the translational degrees of freedom at the node are eliminated and the node becomes an "embedded node". The translational degrees of freedom of the embedded node are constrained to the interpolated values of the corresponding degrees of freedom of the host element [27]. Further details related to the simulation and material properties can be found in a previous work of the authors themselves [19].

2.5 Study of the effect of fiber orientation and distribution

To take into account the influence of fiber distribution on the bearing capacity of the pipe, different fibers clouds (as can be seen in figure 1) were generated for each dosage and each fiber type. As previously stated, the orientation and distribution of them are generated in a completely random way using the Python algorithm mentioned. The algorithm was executed using ABAQUS. Then, the maximum load for each fiber cloud was numerically determined. Since all fiber clouds will be unique due to different fiber distribution and orientation, scatter on the results are expected.

2.6 Parametric study

Eight different combinations of fiber dosage, fiber type and concrete class were studied in order to carry out a parametric study.

To consider the influence of fiber orientation and distribution in the ultimate load as previously explained, five different fiber clouds for each combination were sampled and analyzed.

3 NUMERICAL RESULTS

The mean values for the ultimate load obtained from the five simulations for each combination and their corresponding standard deviation are shown in Table 7 .

Fiber type	Fiber dosage (kg/m3)	Concrete Class	Mean Value (kN)	Standard Deviation (kN)
FF1	15	C30	53.69	0.43
FF1	20	C30	54.67	0.57
FF1	25	C30	55.84	0.51
FF1	30	C30	56.55	0.4
FF3	20	C30	54.98	0.2
FF1	20	C20	48.37	0.2
FF1	20	C25	51.53	0.31
FF1	20	C35	56.81	0.48

Table 7. Mean values and standard desviation of the ultimate load.

In order to validate the model, the results are comapared with the obtained ones in a experimental campaing carried out by the authors themselves. The pipes tested in that campaign were casted with a concrete class C30 containing 20 kg/m^3 of FF1 fibers. A mean value of 60.5 kN was obtained [19]. So, the difference in relation with the numerical results is of around 10%.

In Figure 9 a comparison between the series with the same concrete class and fiber type is made. This table shows the influence of the fiber dosage in the bearing capacity of the pipes.

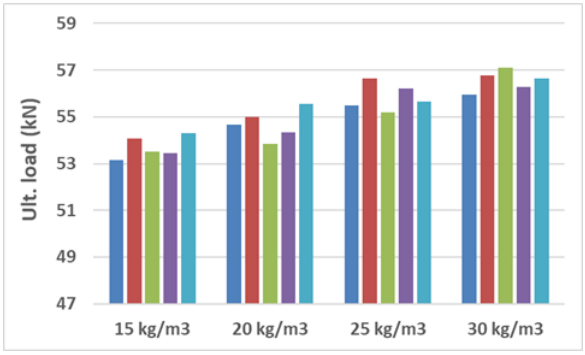

Figure 9. Maximum loads for different fiber dosages. (Concrete class: C30. Fiber Type: FF1.)

As expected, greater the fiber dosage, greater the maximum load in all cases studied. However, the difference, regarding mean values, between the lowest fiber dosage (15 kg/m^3) and the highest fiber dosage (30 kg/m^3) is of 5%.

In figure 10 it can be seen the influence of the concrete class on the ultimate load.

To take into account only the influence of the concrete class, the same fiber clouds were considered, i.e. the five clouds used for these series has exactly the same fiber orientation and distribution. In this case, the difference, in terms of mean values for the ultimate load, between the worst and the better concrete class is around 18 %. Respect to C20, the difference for C25 and C30 are 6.5% and 13% respectively.

Finally, a comparison between series 2 and series 5 is shown in Table 11 with the purpose of assessing the influence of fiber type.

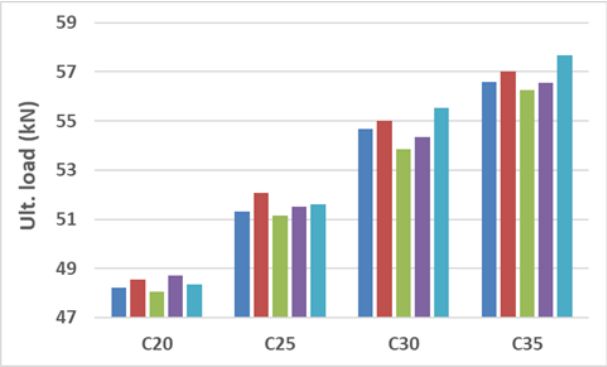

Figure 10. Maximum loads for different concrete classes. (Fiber type: FF1. Fiber dosage: 20 kg/m^3.)

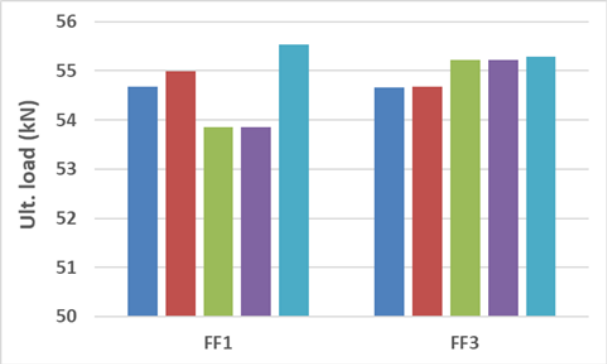

Figure 11. Maximum loads for different fiber types. (Concrete class: C30. Fiber dosage: 20 kg/m^3.)

For the fiber types studied here, the difference is negligible in spite of the fiber clouds for FF3 fiber type has almost the double of fibers than FF1 when the same fiber dosage is considered.

To see the contribution of the fibers, a comparison between the ultimate loads of pipes without fibers and pipes with FF1 fibers, for the different concrete classes adopted, is shown in Table 8.

Concrete Class	Ult. load without fibers (kN)	Mean ult. load with FF1 fibers (kN)	Relative diff. (%)
C20	44.57	48.37	8.5
C25	47.90	51.53	7.5
C30	51.71	54.67	5.7
C35	54.62	56.81	4

Table 8. Ultimate loads of pipes without fibers and pipes containing FF1 fibers. (Fiber dosage: 20 kg/m^3)

As can be seen, the higher concrete class the lower fiber contribution, i.e. the fibers are more useful when the concrete is weaker.

From the failure mode and the cracking pattern observed in the experimental campaign, an analysis considering ideal orientations of fibers are made. This cracking pattern is depicted in Figure 12

The first crack always developed at the inner side of the pipe's invert and crown (red arrows), followed by a crack at the outer side of the pipe's wall of the spring-lines (blue arrow). For this analysis, three different fiber clouds are generated. In the first one, all the fibers are parallel to the X axis, in the second one, they are parallel to the Y axis and in the last one they are parallel to the pipe axis. These orientations are depicted in Figure 13.

For a better visualization only a few fibers were drawn. The ultimate loads obtained for these distributions are shown in Table 9.

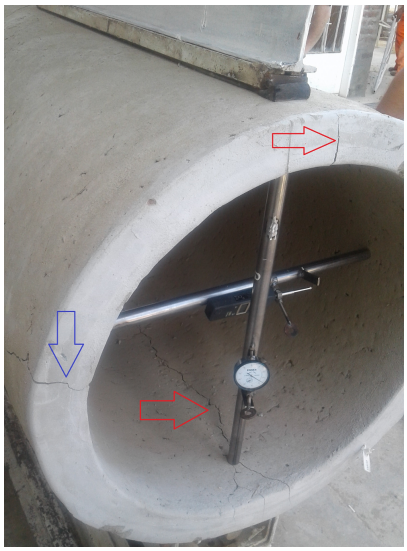

Figure 12. Flexural cracks in a pipe subjected to the TEBT.

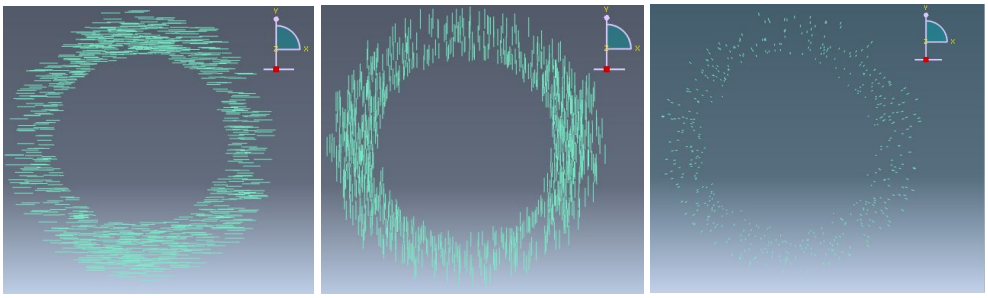

Figure 13. Fiber clouds with predefined orientations. Left: parallel to X axis. Center: parallel to Y axis. Right: parallel to pipe axis.

Fiber orientation	Ultimate load (kN)	Relative diff. in relation to load without fibers (%)
Without fibers	44.57	-
Parallel to X axis	62.79	40.9
Parallel to Y axis	44.91	0.76
Parallel to pipe axis	44.62	0.11

Table 9. Ultimate loads of pipes containing fibers with predefined orientations. (Fiber dosage: 20 kg/m^3. Concrete class: C20.)

As observed, the orientation parallel to the X axis achieved an appreciable increment. This is expected due to, in a flexural member as we have here, the contribution of the fibers to the material strength is more pronounced than otherwise when the alignment of the fibers bridges the crack surfaces. This situation is schematized in Figure 14.

So, the fibers are more effective in crack prevention when they are positioned in a direction normal to the crack plane. The direction of the vector normal to the crack plane is assumed to be parallel to the direction of the maximum principal plastic strain [27]. The direction of the maximum principal plastic strains in a pipe subjected to the TEBT is shown in Figure 15.

As can be seen, the direction of the maximum principal plastic strain coincide with the X axis, like the first predefined fiber orientation considered. For the other two predefined orientations, the fiber contribution was imperceptible.

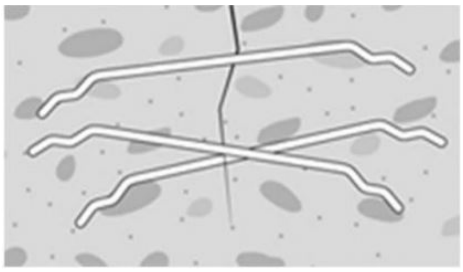

Figure 14. Fibers bridging a crack surface.

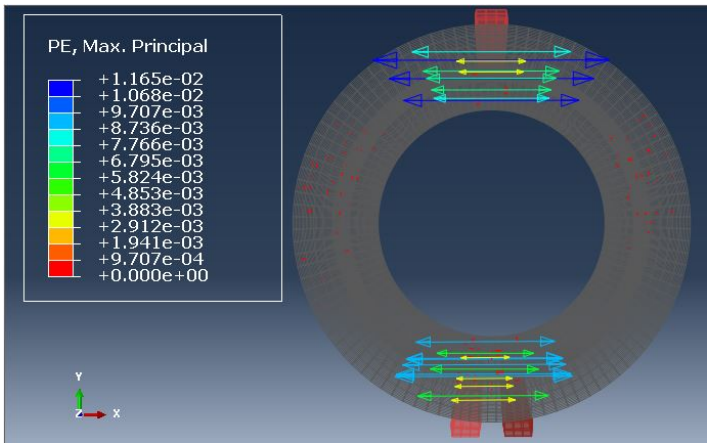

Figure 15. Direction of the maximum principal strains.

4 CONCLUSIONS

In this work, a parametric study of the strength capacity of pipes were performed. Variations in the dosage and type of fibers as well as variations in the concrete class were consider. A 3D model to obtain average probabilistic values of strength capacity of SFRC pipes was presented. The model proposed was used in combination with the Monte Carlo method to perform a probabilistic study of the resistant capacity of the pipes. In order to assess the mechanical performance of SFRC pipes, the three-edge bearing test (TEBT) was simulated. This simulation was carried out in the finite element method analysis tool ABAQUS, where a 2-phase approach was used to model the behavior of SFRC: plain concrete is defined and then the fibers are introduced as wire elements (truss).

From the obtained results we can affirm that the model proposed is more sensitive to changes in the concrete class compared with changes respect to fiber dosage and fiber type. In fact, the model seems to take into account mainly the fiber volume instead of the number of fibers.

In addition, the model represents well fiber contribution when predefined orientations were considered, maximizing the ultimate load when the orientation coincide with the direction normal to the crack plane.

As a further stage, and in order to confirm or improve the proposed model, a deeper assessment containing larger data sets is necessary.

References

[1] De la Fuente, A., Figueiredo, A., Aguado, A., Molins, C., & Chama Neto, P., 2011. Experimentation and numerical simulation of steel fibre reinforced concrete pipes. *Materiales de Construcción*, vol. 61, n. 302, pp. 275–288.

[2] Mohamed, N., Soliman, A., & Nehdi, M., 2014. Full-scale pipes using dry-cast steel fibre-reinforced concrete. *Construction and Building Materials*, vol. 72, pp. 411–422.

[3] Figueiredo, A., De la Fuente, A., Aguado, A., Molins, C., & Chama Neto, P., 2008. Evaluation of the test method for crushing strength of steel fibre reinforced concrete pipes. In *7th International RILEM Symposium on Fibre Reinforced Concrete*.

[4] ASTM, 2015. Standard specification for fiber-reinforced concrete. vol. ASTM C1116.

[5] Laranjeira, F., Grunewald, S., Walraven, J., Blom, C., Molins, C., & Aguado, A., 2011. Characterization of the orientation profile of steel fiber reinforced concrete. *Characterization of the orientation profile of steel fiber reinforced concrete*, vol. 44, n. 6, pp. 1093–1111.

[6] Michels, J., Christen, R., & Waldmann, D., 2013. Experimental and numerical investigation on post cracking behaviour of steel fiber reinforced concrete. *Engineering Fracture Mechanics*, vol. 98, pp. 326–349.

[7] Torrijos, M., Barragán, B., & Zerbino, R., 2010. Placing conditions, mesostructural characteristics and post-cracking response of fibre reinforced self-compacting concretes. *Construction and Building Materials*, vol. 24, n. 6, pp. 1078–1085.

[8] Martinie, L. & Roussel, N., 2011. Simple tools for fiber orientation prediction in industrial practice. *Cement and Concrete Research*, vol. 41, n. 10, pp. 993–1000.

[9] Stahli, P., Custer, R., & Mier, J., 2008. On flow properties, fibre distribution, fibre orientation and flexural behaviour of frc. *Materials and Structures*, vol. 41, n. 1, pp. 189–196.

[10] Laranjeira, F., 2010. *Design oriented constitutive model for steel fiber reinforced concrete*. PhD thesis, Universidad Politécnica de Cataluña,.

[11] Laranjeira, F., Aguado, A., Molins, C., Grunewald, S., Walraven, J., & Cavalaro, S., 2012. Framework to predict the orientation of fiber in frc: a novel philosofy. *Cement and Concrete Research*, vol. 42, n. 6, pp. 752–768.

[12] Zerbino, R., Tobes, J., Bossio, M., & Giaccio, G., 2012. On the orientation of fibres in structural members fabricated with self compacting fibre reinforced concrete. *Cement and Concrete Composites*, vol. 34, n. 2, pp. 191–200.

[13] Grunewald, S., Laranjeira, F., Walraven, J., Aguado, A., & Molins, C., 2012. Improved tensile performance with fiber reinforced self-compacting concrete. *High Performance Fiber Reinforced Cement Composites*, vol. 6, pp. 51–58.

[14] Michels, J., Waldmann, D., Maas, S., & Zurbes, A., 2012. Steel fibers as only reinforcement for flat slab construction experimental investigation and design. *Construction and Building Materials*, vol. 26, n. 1, pp. 145–155.

[15] Gettu, R., Gardner, D., Saldivar, H., & Barragán, B., 2005. Study of the distribution and orientation of fibers in sfrc specimens. *Materials and Structures*, vol. 38, n. 1, pp. 31–37.

[16] Ferrado, F., Escalante, M., & Viviana, R., 2015. Numerical modeling of the mechanical behavior of steel fiber reinforced concrete pipes. In *Proceedings of the XXXVI Iberian Latin-American Congress on Computational Methods in Engineering CILAMCE 2015*.

[17] Ferrado, F., Escalante, M., & Rougier, V., 2016a. Numerical simulation of the three edge bearing test of steel fiber reinforced concrete pipes. *Mecanica Computacional*, vol. XXXIV. Solid Mechanics (A), pp. 2329–2341.

[18] Ferrado, F., Escalante, M., & Rougier, V., 2016b. Análisis estocástico de tubos de hormigón reforzado con fibras de acero: Efecto de la distribución y orientación de las fibras en la capacidad resistente del tubo. *Mecánica Computacional*, vol. 34, n. 54, pp. 3571–3584.

[19] Ferrado, F., Escalante, M., & Viviana, R., 2018. Simulation of the three edge bearing test: 3d model for the study of the strength capacity of sfrc pipes. *Mecánica Computacional*, vol. 36, n. 6, pp. 195–204.

[20] Soetens, T. & Matthys, S., 2014. Different method to model the post-cracking behaviour of hooked-end steel fibre reinforced concrete. *Construction and Building Materials*, vol. 73, pp. 458–471.

[21] Van Gysel, A., 2000. *A. Studie van het uittrekgedrag van staalvezels ingebed in een cementgebonden matrix met toepassing op staalvezelbeton onderworpen aan buiging*. PhD thesis, Ghent University.

[22] Kang, S. & Kim, J., 2011. Investigation on the flexural behavior of uhpcc considering the effect of fiber orientation distribution. *Construction and Building Materials*, vol. 28, n. 1, pp. 57–65.

[23] Barnett, S., Lataste, J., Parry, T., Millard, S., & Soutsos, M., 2010. Assessment of fibre orientation in ultra high performance fibre reinforced concrete and its effect on flexural strength. *Materials and Structures*, vol. 43, pp. 1009–1023.

[24] Vandewalle, L., Heirman, G., & Van Rickstal, F., 2008. Fibre orientation in self-compacting fibre reinforced concrete. In *7th international RILEM symposium on fibre reinforced concrete: design and applications (BEFIB 2008)*, pp. 719–728.

[25] Wille, K. & Naaman, A., 2013. Effect of ultra-high-performance concrete on pullout behavior of high-strength brass-coated straight steel fibers. *ACI Materials Journal*, vol. 110, n. 4, pp. 451–462.

[26] Voo, J. Y. L. & Foster, S. J., 2008. Variable engagement model for fibre reinforced concrete in tension. Technical report, School of Civil and Environmental Engineering, University of New South Wales.

[27] , 2013. Abaqus analysis user's guide. *Dassault Systemes*, vol. 5.